Progress In Electromagnetics Research, PIER 43, 75–100, 2003

A NUMERICAL STUDY OF TM-TYPE SURFACE WAVES ON A GROUNDED DIELECTRIC SLAB COVERED BY A DOUBLY PERIODIC ARRAY OF METALLIC PATCHES

F. Terracher and G. Berginc

Thales Optronique
Rue Guynemer-BP 55, 78283 Guyancourt Cedex, France

Abstract—In this paper we numerically study the propagation of surface waves guided by a metal-backed dielectric slab with biperiodic metallizations on its surface. Such structures are electromagnetic absorbing screens when the dielectric slab is lossy. In this paper, the surface waves are characterized by their longitudinal and transverse wave numbers, which are deduced from the complex pole locations of the reflection coefficient of the screens. The reflection coefficients can be obtained with a moment method. These reflection coefficients are generalized to complex incident wave numbers. The poles are isolated in the complex plane with the help of the argument principle and are calculated with a numerical method based on Müller's algorithm. Then the parametric study of the wave numbers of the surface waves shows that the absorption of an electromagnetic wave by the screens at normal incidence is due to a resonance of the real part of the transverse wave number of the excited surface wave. We also show that there exists a Brewster incidence angle for the absorbing screens with suitable metallization array dimensions. This Brewster angle appears when the pole crosses the branch cut of the two-sheeted Riemann space of the reflection coefficient.

1. INTRODUCTION

Because of their applications in antenna theory, wave scattering, lasers and in fundamental electromagnetic problems, surface waves have been widely studied for the past five decades. A necessary condition for the existence of surface waves is the encounter of an interface by an electromagnetic field during its propagation. The simplest case was first studied by Zenneck in 1907. It was the case of a plane interface separating two perfectly dielectric homogeneous media. We can easily show in that case that for TM polarized electromagnetic wave impinging on the interface under the Brewster angle, the fields have the structure of a wave guided by the interface [1].

G. Goubau [2] and S. S. Attwood [3] have been the first ones to analyze TM-type surface waves propagating over cylindrical conductor of circular cross section and planar conductor covered with a layer of dielectric material. In S. S. Attwood's study, surface waves are assumed to be exponentially decaying fields in the direction normal to and away from the guiding structure. This assumption can be made by the fact that the dielectric layer over the plane conductor is lossless. More recently, a more general study by Ling et al. was presented. In that work the layer is of lossy dielectric and magnetic nature [4]. The method in [4] is formally the same one that in [3] and is based on numerically solving the surface wave dispersion equation.

A theoretical point of view and the study of excitation of surface waves are exposed by L. B. Felsen and N. Marcuvitz in [5]. They show how surface waves are connected with singularities or poles of the reflection coefficient of guiding structures. In [5] is shown how surface wave terms appear when an asymptotic evaluation of the scattered fields is performed. An asymptotic evaluation is used to evaluate integrals whose integrand oscillates at the infinity. Those oscillations make difficult a direct evaluation of the integrals. The integration path

is then deformed to a steepest descent path, which is also a stationary phase path. The value of the integral is then the value of the integrand at the so-called saddle point, and if poles are encountered during the path deformation, the residues of the integral at the pole locations must be added to the result. The pole contributions are then shown to be the surface wave terms. It is important to note that if in asymptotic evaluation of the scattered fields, surface wave terms can be explicitly expressed by the reflection coefficient pole, or, if the scattered fields are not evaluated, a pole in the reflection coefficient of a structure is the signature of a possible surface wave guided by the structure.

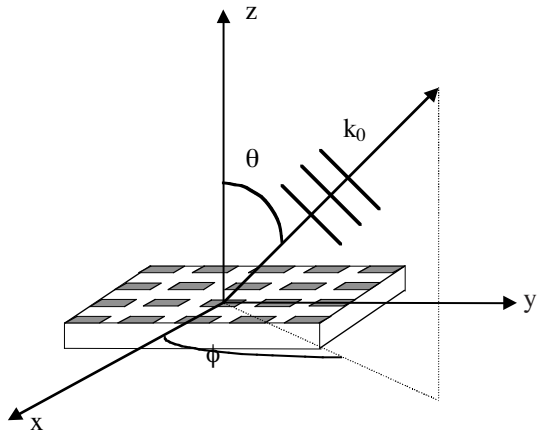

Figure 1. The guiding structure.

In this paper, we study surface waves in doubly periodic absorbing structures. The structures consist of the association of a biperiodic array of metallic patches deposited on a grounded lossy dielectric layer (Fig. 1). In the case of lossy dielectric layer, the structures are electromagnetic absorbing screens. Some surface wave studies have been performed on periodic structures in the past, but these structures were one-dimensional periodical structures. The analytical studies of surface waves was made possible by assuming the width of the strips are small compared to the thickness of the layer, to the period of the structure and to the wavelength [6]. With these assumptions, it is possible to resolve the field equations by making appropriate approximations for the boundary conditions.

In the present paper no such assumption is made, and we study surface waves in biperiodic absorbing structures directly by computing numerically the pole of the reflection coefficient of the structure as we do not have any dispersion equation. The reflection coefficient

computation is based upon an exact prediction method, using Floquet's theorem and a Galerkin method (moment method).

In this paper, we treat in detail the behavior of the surface waves which exist along our heterogeneous structure and the properties of their wave numbers. We describe their relationship to the physical characteristics of the absorption phenomena produced by the biperiodic structure.

Section 2 gives some mathematical definitions. In the section 3, we expose the mathematical background theory used to perform the search of the pole of the reflection coefficient in the complex plane. Section 4 is devoted to the numerical results. We will study the behavior of the surface wave propagation constant when many parameters characterizing the structures vary, like the period of the array, the width of the patches, the permittivity of the dielectric layer, and we show the relationship between the surface wave and the absorption produced by the screens. We work in the microwave domain of frequencies.

2. THEORY

In preparation for studying the surface waves supported by the absorbing structure, we start by giving necessary mathematical preliminaries about the computation of the reflection coefficient of the studied structure, and for the manipulation of the useful complex quantities.

We summarize first the principal feature of all the surface waves varieties, which are supported by planar boundaries. We know that surface waves are propagation modes that appear as characteristic solutions of a boundary-value problem. If the media are lossless, these waves travel longitudinally along the planar boundaries of the stratified configuration. Inside the layers, fields may vary sinusoidally or exponentially with respect to the transverse direction. And, in the exterior region, these fields decay away from the boundaries. Therefore, the surface wave energy is confined inside the bounded layer, and the electromagnetic power flows only along the longitudinal direction. The variation of the field in the upper exterior region is of the form $\exp[i(k_x x - \omega t) - k_z z]$ where k_x and k_z are real and ω is the angular frequency (Fig. 1).

Leaky waves are similar to surface waves because they are also characteristic solutions of boundary-value problems. But leaky waves are characterized by complex k_x and k_z even in a presence of lossless media. For surface waves, k_x and k_z are pure real. For leaky waves, the bulk of their energy is localized in the vicinity of the guiding surfaces

or boundaries. However a small portion of that energy escapes into the upper region (air region) by leaking away at an oblique angle θ_l. Because of the power leakage, all energy is ultimately radiated into the exterior region, the radiation pattern is peaked at the angle θ_l.

Radiation modes are fields that are not tied to the planar boundaries. They propagate at an angle θ with respect to the boundary plane. Unlike surface and leaky waves, the radiation modes form a continuous spectrum with respect to the angular variable θ, the surface and leaky waves are discrete modes. Radiation modes behave as a space wave field, which spreads continuously across the entire θ domain. Surface and leaky waves produce sharp peaks at $\theta = \frac{\pi}{2}$ and θ_l with respect to the normal of planar boundary.

2.1. The Computation of the Reflection Coefficient

We want to calculate the pole of the reflection coefficient of a structure composed of a grounded lossy dielectric slab covered by a doubly periodic array of metallic patches. The numerical scheme can be split up into two principle parts: the first one is about the computation of the reflection coefficient function itself, whose poles we want to calculate; the second one consists in the search of the poles of the reflection coefficient.

On the other hand, we know that the reflection coefficient of any structure can not have a pole for real angles of incidence, or else, that means that the energy reflected by such a structure would be infinite for a finite amount of incident energy. If there is a pole for the reflection coefficient of some structures, it is for a complex incidence angle. So the method for the computation of the reflection coefficient exposed below will be later extended to the case of complex incidence angles.

For the first part, we use an existing Fortran code, which calculates the reflection coefficient of a structure consisting of the association of a biperiodic array of metallic patches and a multilayered absorber (Fig. 1). This code uses a moment method (more exactly a Galerkin method) to calculate the electric current density induced by the incident electric field on the resistive or perfectly conducting patches. The moment method is combined with a Rayleigh method (derived from Floquet's theorem) because the problem is doubly periodic.

We consider a plane wave falling down on a planar, perfectly conducting and infinitely thin array of metallic patches. The array is deposited on a metal-backed lossy dielectric layer (Fig. 1). The array is placed in the $z = 0$ plane. The periodic geometry imposes a periodicity on the incident, scattered and transmitted wave fields near the surface. This periodicity is taken into account by the use of the Floquet's Theorem, so each field can be written as (for example electric

field):

$$\vec{E}(x,y,z) = \sum_{m,n} \vec{E}_{m,n} e^{i(\alpha_m x + \beta_n y \pm \gamma_{mn} z)} \tag{1}$$

$\pm$ corresponds to a propagation along $z > 0$ or $z < 0$.

α_m, β_n and γ_{mn} are propagation constants and are defined by:

$$\alpha_m = k_x + \frac{2m\pi}{p_x} \tag{2}$$

$$\beta_n = k_y + \frac{2n\pi}{p_y} \tag{3}$$

$$\gamma_{mn} = \left(k^2 - \alpha_m^2 - \beta_n^2\right)^{1/2} \tag{4}$$

In this formulation, we assume an $\exp(-i\omega t)$ time dependence of the fields.

In (2)–(4), k_i and p_i are the wave number and the period along i-axis, m and n the Floquet modes. k is the total wavenumber. γ_{mn} is chosen with a positive imaginary part when it is a complex quantity. In this case, we have a damped wave.

Obviously, for the incident fields, only the $(0,0)$ principal mode propagates. As patches are perfectly conducting, the incident electric field induces an electric current density $\vec{J}$, which itself induces a vector potential $\vec{A}$. Both of them are related by the following equation

$$\vec{A}(x,y,z) = \iint \vec{J}(x',y') \overline{\overline{G}}(x,y,z|x',y') dx' dy' \tag{5}$$

where $\overline{\overline{G}}$ is the free-space Green's function.

The electric field is related to the potential vector by

$$\vec{E}^{scat} = -i\omega \left\{ \vec{A} + \frac{1}{k^2} \vec{\nabla}(\vec{\nabla} \cdot \vec{A}) \right\} \tag{6}$$

Eq. (6) is the electric field integral equation (EFIE).

In a matrix form and in the spectral domain, Eq. (6) can be rewritten as

$$\begin{bmatrix} \tilde{E}_x^{scat} \\ \tilde{E}_y^{scat} \end{bmatrix} = -\frac{1}{j\omega\varepsilon_0} \begin{bmatrix} k_0^2 - \alpha^2 & -\alpha\beta \\ -\alpha\beta & k_0^2 - \beta^2 \end{bmatrix} \tilde{\overline{\overline{G}}}(\alpha,\beta) \tilde{\vec{J}}_t(\alpha,\beta) \tag{7}$$

$\tilde{\vec{J}}_t$ is the tangential electric current density in the spectral domain, and $\tilde{\overline{\overline{G}}}$ is the free-space Green's function in the spectral domain.

Taking the inverse transform of Eq. (7), and enforcing the boundary condition $\vec{E}^{inc} = -\vec{E}^{s}$ on the conducting patches, Eq. (7) reads now

$$\begin{bmatrix} E_x^{inc} \\ E_y^{inc} \end{bmatrix} = \frac{1}{j\omega\varepsilon_0} \iint \begin{bmatrix} k_0^2 - \alpha^2 & -\alpha\beta \\ -\alpha\beta & k_0^2 - \beta^2 \end{bmatrix} \tilde{\tilde{G}}(\alpha,\beta)\tilde{\vec{J}}_t(\alpha,\beta)e^{j\alpha x}e^{j\beta y}d\alpha d\beta \tag{8}$$

As the structure is biperiodic, the current has a discrete spectrum in the Fourier domain, i.e., $\alpha = \alpha_m$ and $\beta = \beta_n$, so we have

$$\begin{aligned} \begin{bmatrix} E_x^{inc} \\ E_y^{inc} \end{bmatrix} &= \frac{1}{j\omega\varepsilon_0 a_x a_y} \sum_m \sum_n \begin{bmatrix} k_0^2 - \alpha_m^2 & -\alpha_m\beta_n \\ -\alpha_m\beta_n & k_0^2 - \beta_m^2 \end{bmatrix} \\ &\quad \tilde{\tilde{G}}(\alpha_m,\beta_n) \begin{bmatrix} \tilde{J}_x(\alpha_m,\beta_n) \\ \tilde{J}_y(\alpha_m,\beta_n) \end{bmatrix} e^{j\alpha_m x}e^{j\beta_n y} \end{aligned} \tag{9}$$

Eq. (9) demonstrates that we first have to calculate the induced electric current density on the patches to know the scattered electric field. This calculation is carried out using a Galerkin method. Details and references for the calculation are given in [7, 8].

As the code was first written for real incidence angles, some modifications were added to allow complex incidence angles. The sign of the propagation constants were modified to take into account the region of the complex plane where the computation is performed, as we shall show in the next section.

2.2. The Propagation Constant

As we previously said in the introduction, the problem is of biperiodic nature. Floquet's theorem is useful in the computation of the reflected fields. Thus, we first define the transverse wave number of Floquet's modes.

If the direction of the incident wave number $\vec{k}_0$ is defined by the angles θ and ϕ as shown on Figure 1, then the propagation constant γ_{mn} of each (m,n) Floquet mode is given by

$$\gamma_{mn}^2 = k_0^2 - k_{xm}^2 - k_{yn}^2 \tag{10}$$

where k_{xm} and k_{yn} are the longitudinal wave numbers components of the (m,n) Floquet mode, and are given by

$$k_{xm} = k_0 \sin\theta\cos\phi + m\frac{2\pi}{a}, \tag{11a}$$

$$k_{yn} = k_0 \sin\theta\sin\phi + n\frac{2\pi}{a}. \tag{11b}$$

In Equations (11a)–(11b), a is the period of the doubly periodic array of metallic patches (we assume the cells have a square shape).

In this paper, for the sake of simplicity we assume that the angle ϕ is zero. The study is then confined to the computation of only the x-component of the wave number in the complex plane.

The code used in this study was previously written for real incidence angles θ. As we said, it is necessary to extend the definition of the wave numbers to complex angles. Therefore the complex θ angle is given by

$$\theta = \theta_r + i\theta_i \tag{12}$$

where θ_r and θ_i are respectively the real part and the imaginary part of the complex incidence angle. In that case, the real sine function in (11a)–(11b) becomes complex:

$$\sin(\theta) = \sin\theta_r \cosh\theta_i + i\cos\theta_r \sinh\theta_i \tag{13}$$

Hence, we obtain the complex propagation constant taking the square root of (10).

2.3. Definition of the Complex Square Root Function

The argument of the square root of (10) is now a complex argument, so we need to give a coherent definition of it. We rewrite first the transverse wave number as

$$\gamma = \left(k_0^2 - \zeta^2\right)^{1/2} \tag{14}$$

where ζ is the longitudinal wave number.

We need to search for the transverse wave number associated with a pole in a complex plane. But in the complex plane, the square root is a double-valued function. To make the definition of γ unique, a two-sheeted complex plane ζ is necessary, with branch cuts providing the means of passing from one Riemann sheet to the other. The selection of branch cuts is arbitrary but determines the disposition of those regions of the complex ζ plane in which $\mathrm{Im}(\gamma) > 0$, or $\mathrm{Im}(\gamma) < 0$.

In our case, the harmonic time dependence of the fields is $\exp(-i\omega t)$. Thus, the imaginary part of γ should be positive to ensure the fields remain bounded at infinity.

Another condition is imposed on γ. When ζ is real and $|\zeta| < k_0$, the wave is propagating, and the transverse wave number should be real and positive (thus there is a bulk wave, and no more a surface wave).

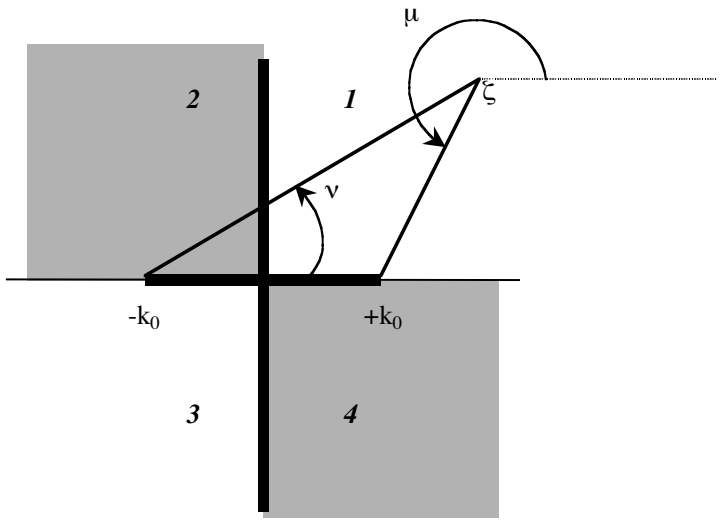

Figure 2. Branch cuts in the complex ζ plane. Branch cuts follow the $\mathrm{Im}(\gamma) = 0$ contour.

To satisfy those conditions, the branch cuts are placed along the contour $\mathrm{Im}(\gamma) = \gamma'' = 0$. The square root function is then defined by the following means. Let us consider,

$$\begin{aligned} (k_0 - \zeta) &= |k_0 - \zeta| e^{i\mu} \\ (k_0 + \zeta) &= |k_0 + \zeta| e^{i\nu} \end{aligned} \tag{15}$$

where μ and ν are two real numbers, and are equal to zero when $-k_0 < \zeta < +k_0$, and are selected as shown in Figure 2. Hence,

$$\gamma = \left(k_0^2 - \zeta^2\right)^{1/2} = \left|\left(k_0^2 - \zeta^2\right)^{1/2}\right| \cdot e^{i(\mu+\nu)/2}. \tag{16}$$

With this definition, and with the branch cuts we have chosen, the imaginary part of γ is positive on the entire top Riemann sheet, which is the physical sheet. The real part of γ is positive on the shaded region of the top sheet, as shown in Figure 2. On the second sheet, the sign of the real and imaginary parts are reversed.

Such a rigorous definition of the complex square root function is necessary to ensure the coherence of the computation in the complex plane. Other choices for the branch cuts are possible, and we refer the reader to [9] for more details.

Another transformation is useful to conduct the computation in a simple way. It is more convenient to search a pole in the complex

angle θ plane rather than in the complex ζ plane. To that end, we use the transformation

$$\zeta = k_0 \sin\theta \tag{17}$$

where θ is a complex angle. When we separate (8) into its real and imaginary parts, we have

$$\begin{aligned} \zeta_r &= k_0 \sin\theta_r \cosh\theta_i \\ \zeta_i &= k_0 \cos\theta_r \sinh\theta_i \end{aligned} \tag{18}$$

Hence,

$$\gamma = k_0 \cos\theta = k_0(\cos\theta_r \cosh\theta_i - i \sin\theta_r \sinh\theta_i) \tag{19}$$

where we wrote $\theta = \theta_r + i\theta_i$.

The transformation (17) has some advantages. This representation is more convenient when we perform calculation of the diffracted fields by the structure with an asymptotic method. Thus the four quadrants in the ζ plane map in the θ-plane into corresponding regions via equation (18) as shown in Figure 3.

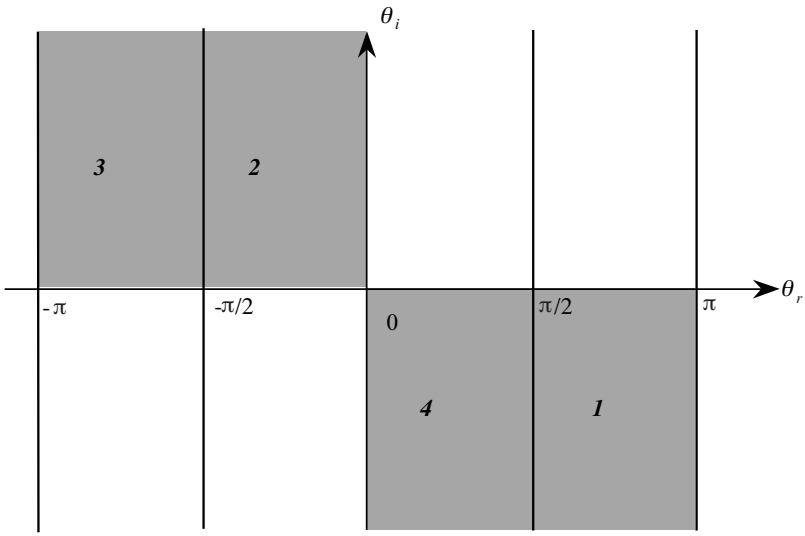

Figure 3. Mapping from the complex θ plane to the complex ζ plane.

2.4. The Complex Reflection Coefficient

Now we give a definition for the complex reflection coefficient. As the different components of the electromagnetic field are naturally

complex quantities, the complex efficiency of the structure can be easily expressed as a function of them,

$$\tilde{eff} = \frac{E_{rx} \cdot \overline{H}_{ry} - E_{ry} \cdot \overline{H}_{rx}}{E_{ix} \cdot \overline{H}_{ix} - E_{iy} \cdot \overline{H}_{ix}} \tag{20}$$

where E_{rx}, E_{ry}, H_{rx}, H_{ry} (resp. E_{ix}, E_{iy}, H_{ix}, H_{iy}) are the components of the specular (incident) electric and magnetic fields. The symbol $\overline{H}$ indicates a complex conjugate quantity. As the period array is chosen less than the incident wave wavelength, the central Floquet's mode (the specular ray) only propagates and we define the complex reflection coefficient by the equation (20).

3. THE SEARCH OF POLE IN THE COMPLEX PLANE

In this section we expose the mathematical aspect of the method used to efficiently search the pole of the structure in the complex plane.

It is easy to find a pole (or zero) for an analytical function. When the function is a pure numerical function, the computation is quite easy in the case of one variable. In the present situation, there are two real variables, θ_r and θ_i the real and the imaginary part of the complex angle. Even if some routines exist in scientific library like IMSL or Lapack, it is interesting for the computer scientist to know the principles of the method. Here we concentrate our attention on the part of the method which deals with the proof of the existence of poles in the complex plane because in each method, an iterative search is stopped when the modulus of the argument is less (for a zero) or greater (for a pole) than an arbitrary small or large value. But the validity of such a condition can not prove that the calculated point is a zero or a pole for the function, the condition proves only we have an extremum.

Fortunately, complex analysis gives us a solution, called argument's principle. We give here the requisite theorems.

Theorem 1

Let us consider a meromorphic function f in a domain D, and a sub-domain G of D, the frontier of G containing neither pole nor zero. If N is the number of zeroes for f and P is the number of poles for f into the sub-domain G (we take into account the order of the zero and the pole), then we have

$$N - P = \frac{1}{2i\pi} \int_{\partial G} \frac{f'(z)}{f(z)} dz. \tag{21}$$

Theorem 2 (Argument principle)

With the theorem 1 conditions, we have

$$N - P = \frac{1}{2\pi}\Delta_{\partial G} Arg(f), \tag{22}$$

where $\Delta_{\partial G} Arg(f)$ denotes the growth in the argument of f along the frontier of G. The proofs are easy and interested reader can find them in any mathematical book, like [10] for example.

This second theorem allows us to perform numerically the proof of the existence of a pole for the reflection coefficient. N-P is the number of rotations of the vector $f(z)$ around the origin when z runs along the frontier of G.

So if we scan a region of the complex plane where there is no zero for the reflection coefficient, then $N = 0$ and we then get immediately the number P of poles inside the domain. As the number P of poles is calculated with the order of each pole, if we found that P equals one, we have the result of the existence of a unique pole inside the domain.

We can note that Eq. (22) gives only the difference between the number N of zeroes and the number P of poles in the domain. As we only look for the poles, we have to do the hypothesis that there is no zero in the region of the complex plane we scan. Then Eq. (22) gives the number of poles. It is a strong hypothesis but we are helped in mapping the modulus of the reflection coefficient to see if there is a possibility for the existence of one or more zero. If there is not, Eq. (22) gives the number of poles, else we have to define a smaller domain of the complex plane to isolate the zero out of it.

For a numerical point of view, as it is numerically easier to find a zero than a pole, when we look for a pole for the reflection coefficient we search the complex zero of the inverse of the reflection coefficient, with a numerical method based on Müller's algorithm.

4. NUMERICAL RESULTS

In this section we show numerical results for the pole of TM type surface wave. The structure is the following: a biperiodic array of metallic patches is deposited on a dielectric metal-backed substrate (Fig. 1).

We show the dependence of the surface wave propagation constant with numerous parameters, like the period of the array, the dimension of the metallic patches, the dielectric permittivity of the slab. In this section, the dielectric constant is kept constant for an easier interpretation of the results.

The methodology is the following:

1. We first begin by a particular case: we look for the pole of a perfect dielectric open waveguide. In that case, we do not use the moment method as the array of patches is removed. Indeed in the case of an open waveguide, an analytical expression exists for the TM reflection coefficient. So we look for the pole of that expression. It is what we call the trivial solution.
2. We then consider a perfect dielectric open waveguide covered by an array of very small metallic patches. As the patches are very small, they act as a small perturbation for the structure in a way that we can find the pole of the reflection coefficient for this new structure near the one of the open waveguide without the metallic patches. In that case we have now to use the method of moments to calculate the reflection coefficient because an analytical expression no more exists.
3. Then we can follow the path of the pole in the complex plane when we make undergo small variations to the parameters of the structure like the losses in the dielectric layer, the period of the array or the size of the metallic patches. Obviously, the method of moment is used again.

4.1. The Solution in a Trivial Case: Dielectric Lossless Metal-Backed Slab

Rather than begin the study with an arbitrary geometry for the array, we first remove the biperiodic array from the structure. Thus we get a simple guiding slab structure. To achieve simplification, we choose a real dielectric constant. Hence, the structure is now reduced to an open waveguide of slab type. For this particular kind of structure, we do not need any complicated numerical code to compute the reflection coefficient for which we have the following analytical expression in TM polarization [9] :

$$r(\theta) = \frac{\sqrt{\varepsilon_r - \sin^2\theta}\sin\left(kt\sqrt{\varepsilon_r - \sin^2\theta}\right) - i\varepsilon_r\cos(\theta)\cos\left(kt\sqrt{\varepsilon_r - \sin^2\theta}\right)}{\sqrt{\varepsilon_r - \sin^2\theta}\sin\left(kt\sqrt{\varepsilon_r - \sin^2\theta}\right) + i\varepsilon_r\cos\left(\theta\right)\cos(kt\sqrt{\varepsilon_r - \sin^2\theta}\right)} \tag{23}$$

where ε_r is the relative dielectric constant

t is the slab thickness,

k is the wave number in vacuum,

θ is the incidence angle.

In that case, surface wave solutions lie in particular region, as shown in Figure 4. In the complex angle plane, the pole solutions are

$$\theta_p = +\frac{\pi}{2} - i\theta_i, \quad \text{or} \quad \theta_p = -\frac{\pi}{2} + i\theta_i. \tag{24}$$

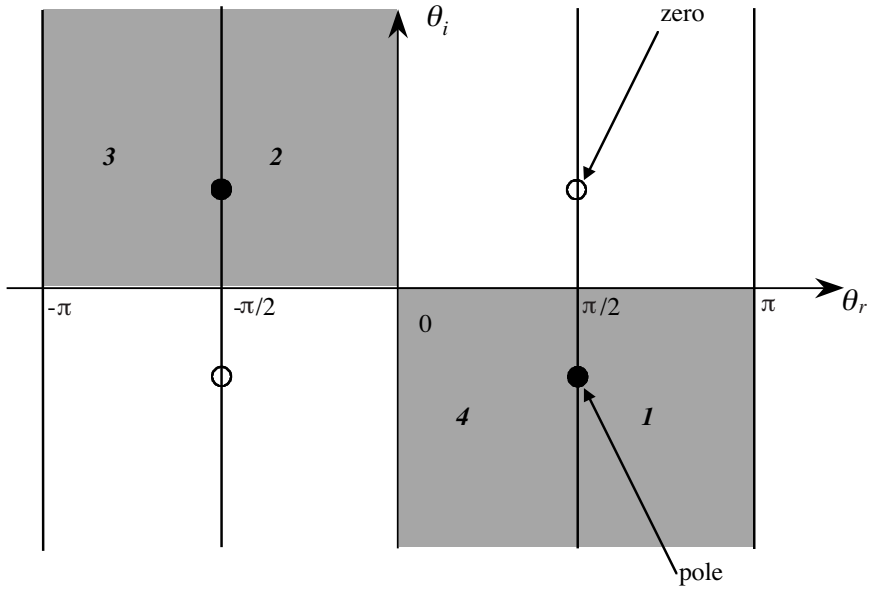

Figure 4. Pole and zero locations in the lossless case (complex angles plane).

with $\theta_i > 0$.

These solutions are the zeroes of the denominator of Eq. (23).

θ_p corresponds to a wave guided by the slab. This guided wave is of evanescent nature above the dielectric interface. This kind of waves has been widely described in the past even in the case of lossy dielectric [1, 3, 9, 11], or in the case where the substrate is magnetic [4, 12].

An interesting remark can be made about the position of zeroes and poles in the complex angle plane for the present structure. To that end, let us write the reflection coefficient onto the axes $\pm\frac{\pi}{2} + i\theta_i$.

On the $+\frac{\pi}{2} - i\theta_i$-axis we have

$$r^+(\theta) = \frac{\sqrt{\varepsilon_r - \cosh^2\theta_i}\,\sin\left(kt\sqrt{\varepsilon_r - \cosh^2\theta_i}\right) - \varepsilon_r \sinh(\theta_i)\cos\left(kt\sqrt{\varepsilon_r - \cosh^2\theta_i}\right)}{\sqrt{\varepsilon_r - \cosh^2\theta_i}\,\sin\left(kt\sqrt{\varepsilon_r - \cosh^2\theta_i}\right) + \varepsilon_r \sinh(\theta_i)\cos\left(kt\sqrt{\varepsilon_r - \cosh^2\theta_i}\right)} \tag{25a}$$

and on the $-\frac{\pi}{2} + i\theta_i$-axis

$$r^-(\theta) = \frac{\sqrt{\varepsilon_r - \cosh^2\theta_i}\sin\left(kt\sqrt{\varepsilon_r - \cosh^2\theta_i}\right) + \varepsilon_r \sinh(\theta_i)\cos\left(kt\sqrt{\varepsilon_r - \cosh^2\theta_i}\right)}{\sqrt{\varepsilon_r - \cosh^2\theta_i}\sin\left(kt\sqrt{\varepsilon_r - \cosh^2\theta_i}\right) - \varepsilon_r \sinh(\theta_i)\cos\left(kt\sqrt{\varepsilon_r - \cosh^2\theta_i}\right)} \tag{25b}$$

From (25a) and (25b), we have the following relations

$$r^+(\theta_i > 0) = \frac{1}{r^-(\theta_i > 0)} \tag{26a}$$

$$r^+(\theta_i < 0) = \frac{1}{r^-(\theta_i < 0)} \tag{26b}$$

$$r^+(\theta_i > 0) = r^-(\theta_i < 0) \tag{26c}$$

$$r^+(\theta_i < 0) = r^-(\theta_i > 0) \tag{26d}$$

The relations (26a)–(26d) allow us to conclude to the existence of a zero for the reflection coefficient of the lossless structure on the second Riemann sheet when a pole is located on the physical sheet, as indicated on the Figure 4. Moreover, we have

$$\theta_z = \overline{\theta}_p \tag{27}$$

where θ_z is the zero of the reflection coefficient.

4.2. Lossless Dielectric Slab Coated by a Doubly Periodic Array of Metallic Patches

In this section, we study the propagation constant of surface waves in the case of a lossless metal-backed dielectric coated by a biperiodic array of metallic patches. As we know the location of the pole for the reflection coefficient in the case where the array is absent, we start by the introduction of small patches, which constitute a small perturbation of the initial structure. Hence, a small perturbation in the propagation constant of the surface waves should be observed. As we can see in Figure 5, the wave number remains real after the introduction of the metallic patches. In all this paper, the wave number and propagation constants are normalized to the wave number k_0. In Figure 6, we show the wave number k as a function of the metal-free surface of the array, for four values of the array period. We observed that for very small patches ($d/a \to 0.5$; d being the half

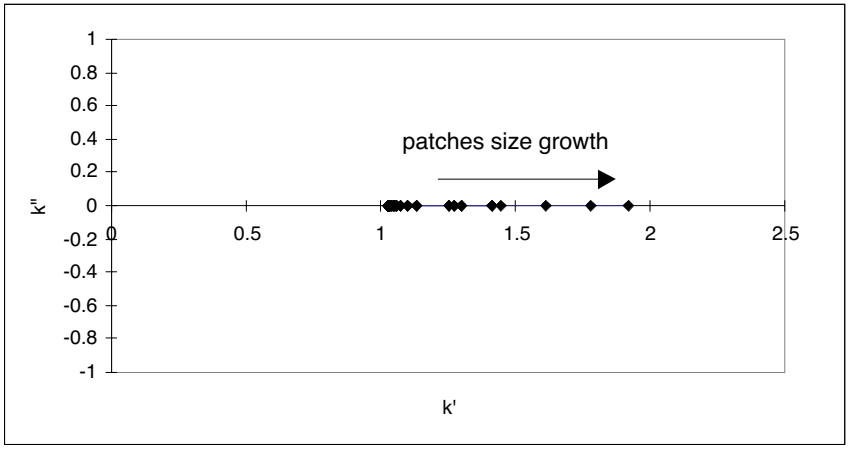

Figure 5. Longitudinal wave number as a function of the patches size. Dielectric layer thickness is 3 mm. $\varepsilon'_r = 5.81$ (lossless case), frequency is 4 GHz. Array period is 15 mm.

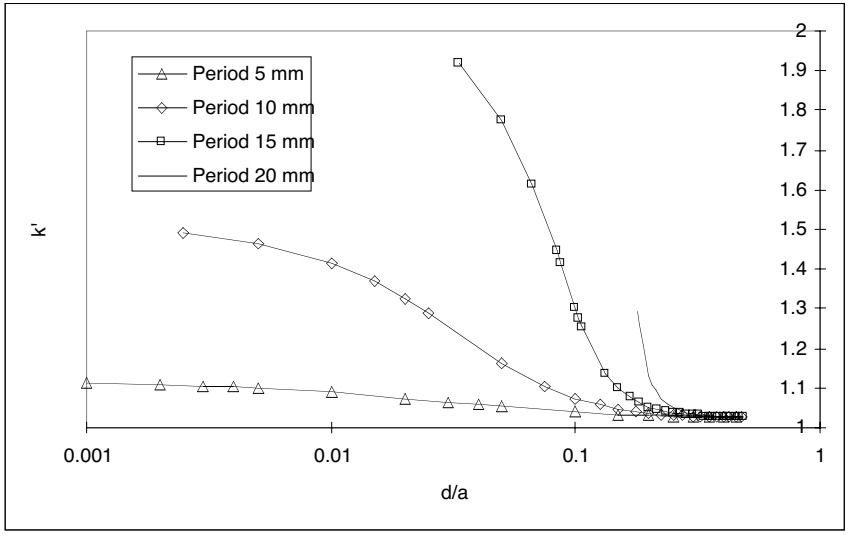

Figure 6. Longitudinal wave number with the patches size for several values of the array period. $\varepsilon'_r = 5.81$ (lossless case). Dielectric layer thickness is 3 mm, frequency is 4 GHz.

spacing between the patches and a the array period) k remains near its value for the lossless dielectric metal-backed slab, as we previously said, before increases for large metallic patches. We also note that the value of the period is an important parameter: as for small periods, the wave number values vary very slowly, and for large periods, the wave number value is sharply increasing. In the case of lossy dielectric, for the reflection coefficient, no important effect is observed as the period of the array and the size of the patches remain small in comparison with the incident wavelength.

4.3. General Case

In this section we study the case where the substrate is a lossy dielectric. We analyze the influence of the imaginary part of the dielectric constant, and the geometrical parameters of the structure, first for a fixed frequency, and then as a function of the frequency. In all the results presented below, the thickness of the screen is kept constant. It is clear that the position of the poles in the complex plane depends on the thickness of the dielectric layer. For example, the trivial solution for the open waveguide depends on the thickness t of the dielectric slab (see Eq. (23)).

In Figure 7 and Figure 8, we show the real and imaginary parts of the wave number of the surface wave, as a function of the dielectric losses, for four values of the patches dimensions, the array period being fixed to 15 mm. As a matter of fact, when the dielectric constant is no more real, the wave number and the propagation constant associated to the surface wave become complex numbers. As we can see, both of the parts are clearly resonant. Their resonant behavior is most pronounced when the patches fill almost entirely individual cells. This resonant character is obviously observed for the propagation constant too (Figures 9 and 10). We can also note that when the dielectric losses become infinite, the structure becomes a metallic interface and the wave number tends to k_0.

In the case where the dielectric layer is lossy ($\varepsilon = 4.81 + 1.82i$) the Figures 11 and 12 show the longitudinal wave number when the conducting patches increase in size, for four values of the array period. The frequency is fixed to 4 GHz. In this case, we can note that for two cases, the imaginary part of the longitudinal wave number becomes negative for a sufficiently large patch size. This is more visible in Figure 13 where the trajectory of the longitudinal wave number is shown in the complex k plane. Two curves (those for which the array period is equal to 12 and 15 mm) cut the real normalized longitudinal wave number axis at a location less than unity. This means that the poles cross the branch cut of the two-sheeted Riemann space to go into the second

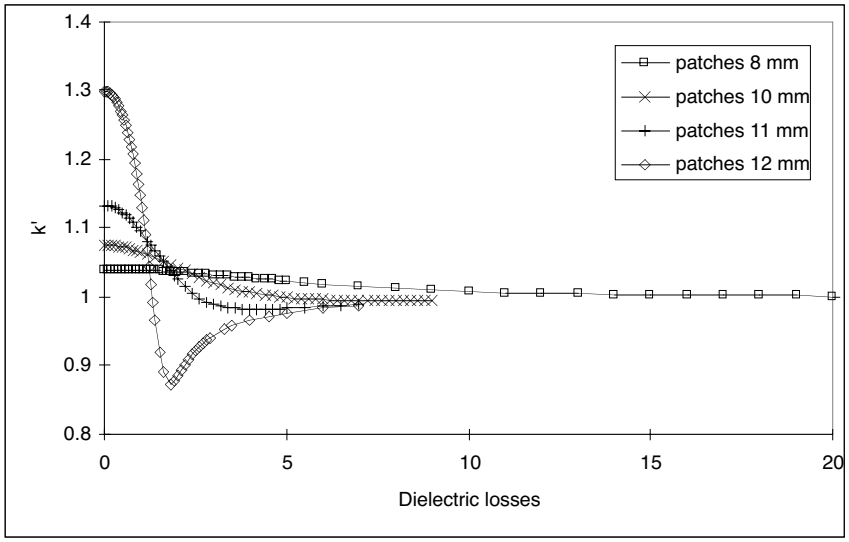

Figure 7. Longitudinal wave number (real part). Dielectric layer thickness is 3 mm, $\varepsilon'_r = 5.81$, frequency 4 GHz. Array period 15 mm.

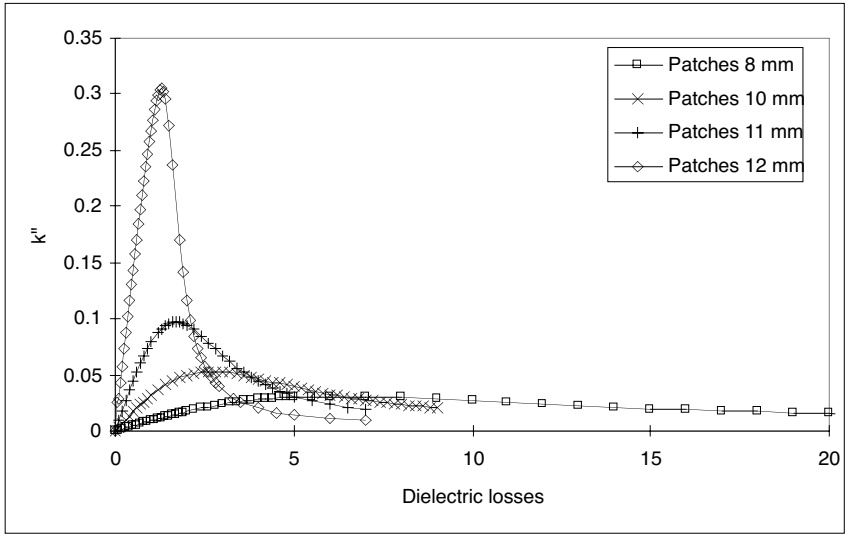

Figure 8. Longitudinal wave number (imaginary part). Dielectric layer thickness is 3 mm, $\varepsilon'_r = 5.81$, frequency 4 GHz. Array period 15 mm.

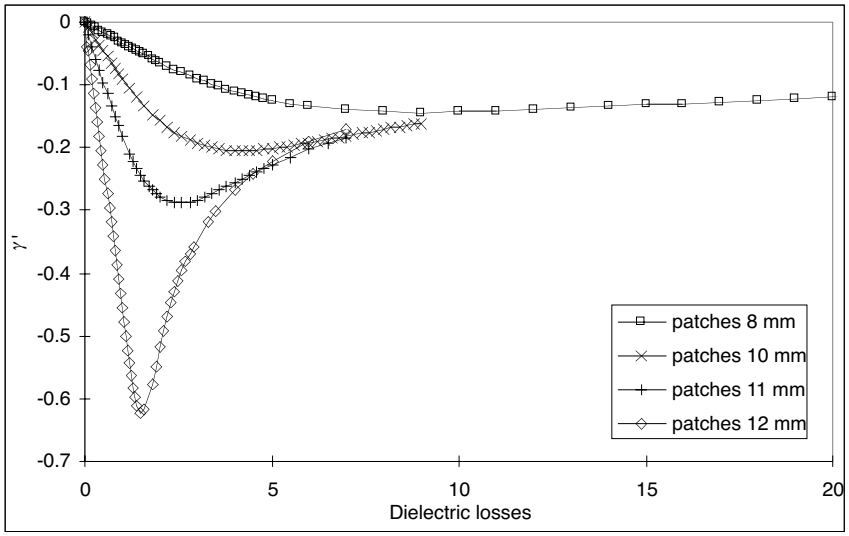

Figure 9. Transverse wave number (real part). Dielectric layer thickness is 3 mm, $\varepsilon'_r = 5.81$, frequency 4 GHz. Array period 15 mm.

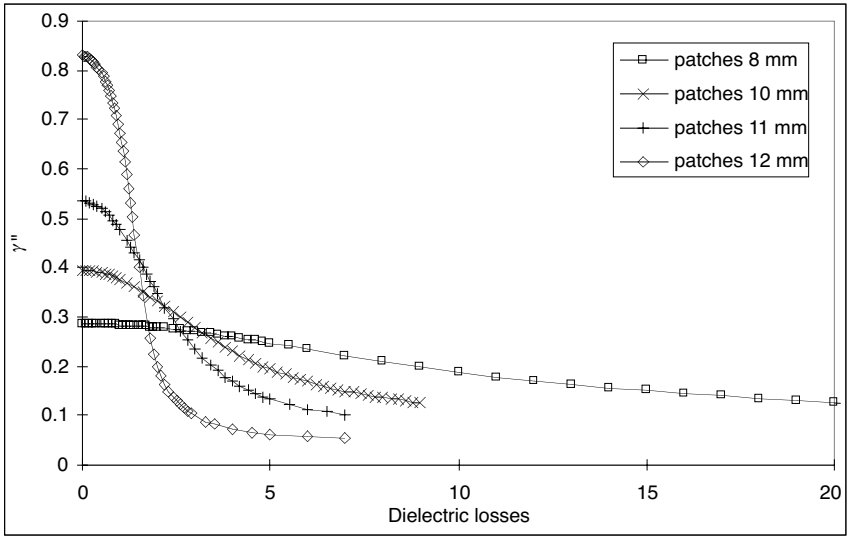

Figure 10. Transverse wave number (imaginary part). Dielectric layer thickness is 3 mm, $\varepsilon'_r = 5.81$, frequency 4 GHz. Array period 15 mm.

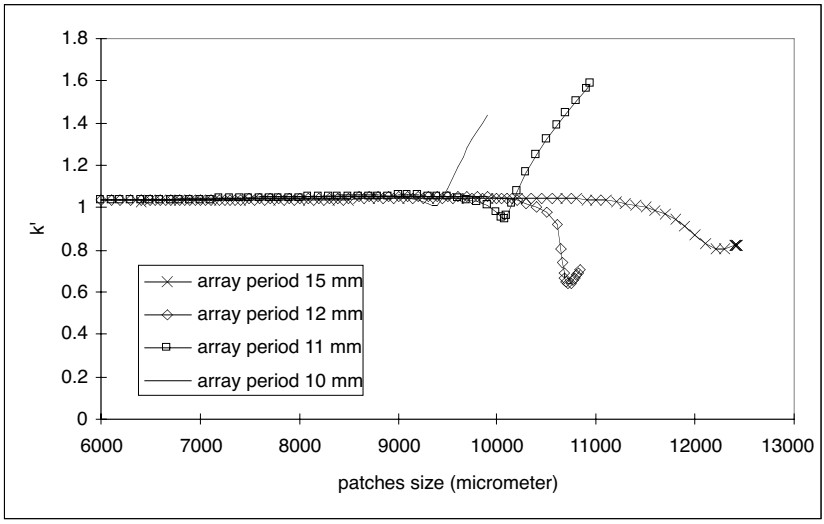

Figure 11. Longitudinal wave number (real part). Dielectric layer thickness is 3 mm, $\varepsilon_r = 5.81 + 1.82i$, frequency 4 GHz.

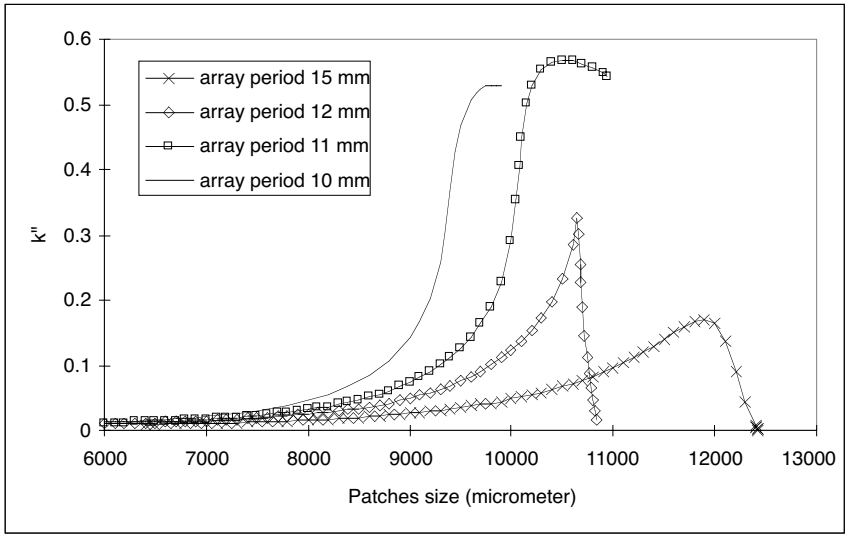

Figure 12. Longitudinal wave number (imaginary part). Dielectric layer thickness is 3 mm, $\varepsilon_r = 5.81 + 1.82i$, frequency 4 GHz.

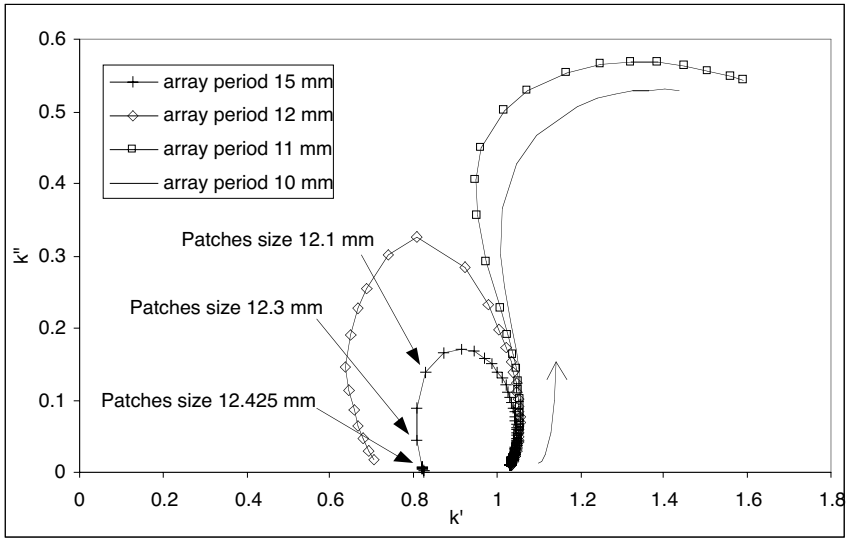

Figure 13. Trajectory of the pole in the complex k plane. Patches growing in size. Dielectric layer thickness is 3 mm, $\varepsilon_r = 5.81 + 1.82i$, frequency 4 GHz.

Riemann sheet (where $\gamma'' < 0$). Then in the region 4 of the physical Riemann sheet (Fig. 2), there is a zero for the reflection coefficient, and especially on the real normalized longitudinal wave number axis, since the definition of the square root function we have taken is such as $\gamma' > 0$ for $k'' = 0$ on the physical sheet. The change of the Riemann sheet can be interpreted as a cut for the guided mode.

On the real k' axis, the zero of the reflection coefficient can then be characterized by a longitudinal wave number which is equal to

$$k = k' = k_0 \sin\theta_r < k_0 \tag{28}$$

where k_0 is the incident wave number and θ_r a real incidence angle for the electromagnetic wave. θ_r is a Brewster angle under which the reflectivity of the structure is zero, for a TM polarized incident wave.

From (19), the Brewster angle is given by

$$\sin\theta_r = \frac{k'}{k_0} \tag{29}$$

Practically, the longitudinal wave numbers being normalized with respect to k_0, they directly give the value of the sine of the Brewster angle with the associated patch size. For example, in Figure 13, in the

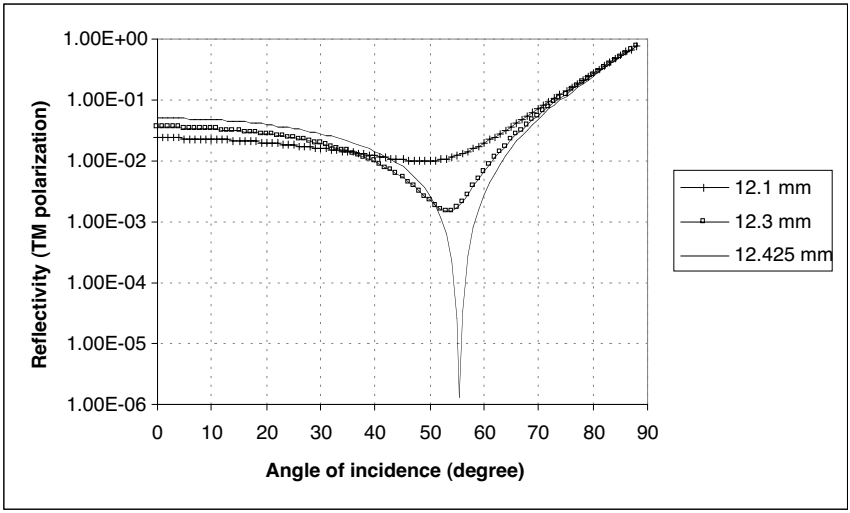

Figure 14. Reflectivity of an absorbing screen as a function of the incidence angle, TM polarization. Dielectric layer thickness is 3 mm, $\varepsilon_r = 5.81 + 1.82i$, array period 15 mm, patches size 12.425 mm, frequency 4 GHz.

case of a 15 mm array period, the Brewster angle of the structure is equal to 55.5° for 12.425 mm patches sized. Moreover, Figure 14 shows the reflectivity of such an absorbing structure, as a function of the incidence angle, in TM polarization. We can see that the reflectivity is equal to zero for an angle of incidence equals to 55.5°.

Figure 14 also shows the reflectivity of the structure when the metallic patches are smaller in size than 12.425 mm. As we can see, while the pole of the reflection coefficient stays far-off the branch cut (see Figure 13), the reflectivity of the structure does not have any zero for any angle of incidence. At the most we can observe a minimum in the reflectivity, which is the mark of the existence of a pole somewhere in the complex plane in the vicinity of the branch cut.

When the frequency is no more constant, Figures 15 and 16 show the real and imaginary parts of the longitudinal wave number of the guided mode, for six patch sizes in 15 mm square cells. Clearly, they behave like the ones shown in Figures 11 and 12, we can notice some maxima for their imaginary part and minima for their real part.

Moreover, we show in Figure 17 the frequency of the minimum of the reflectivity of the absorbing screen when it is illuminated by a plane wave at normal incidence, as a function of the maximum of the real part of the transverse wave number γ' of the guided

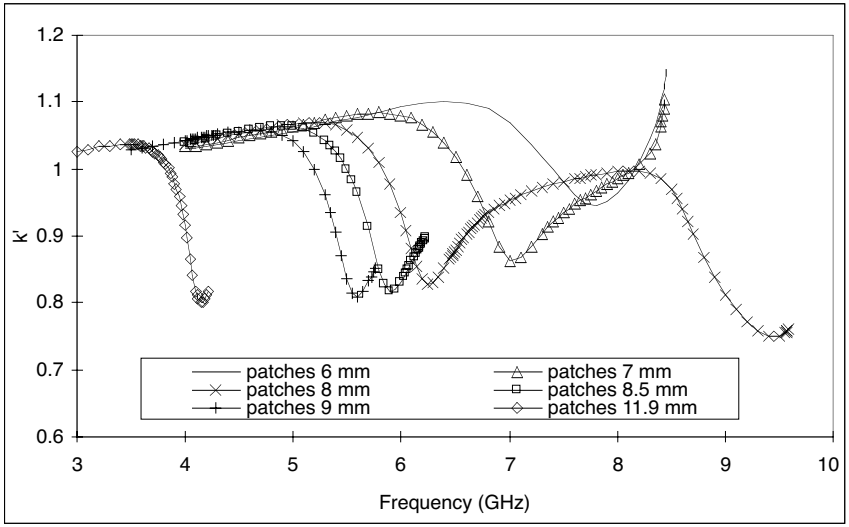

Figure 15. Longitudinal wave number (real part). Dielectric layer thickness is 3 mm, $\varepsilon_r = 5.81 + 1.82i$, array period 15 mm.

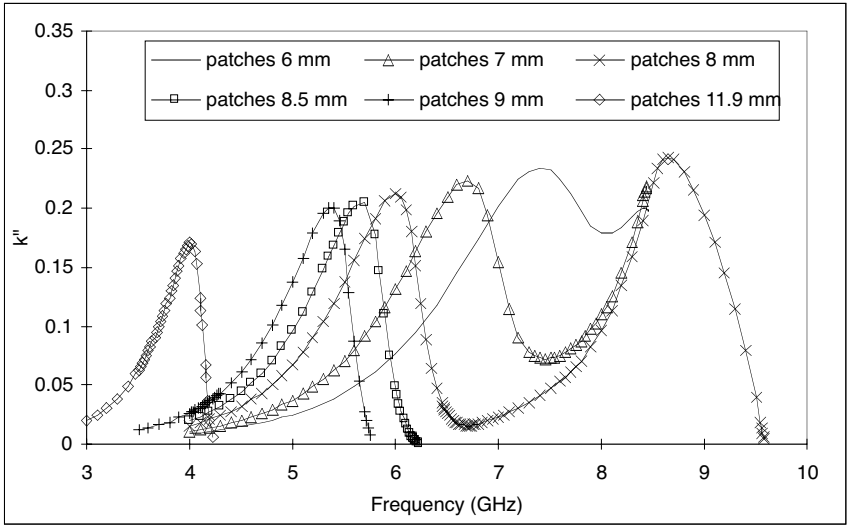

Figure 16. Longitudinal wave number (imaginary part). Dielectric layer thickness is 3 mm, $\varepsilon_r = 5.81 + 1.82i$, array period 15 mm.

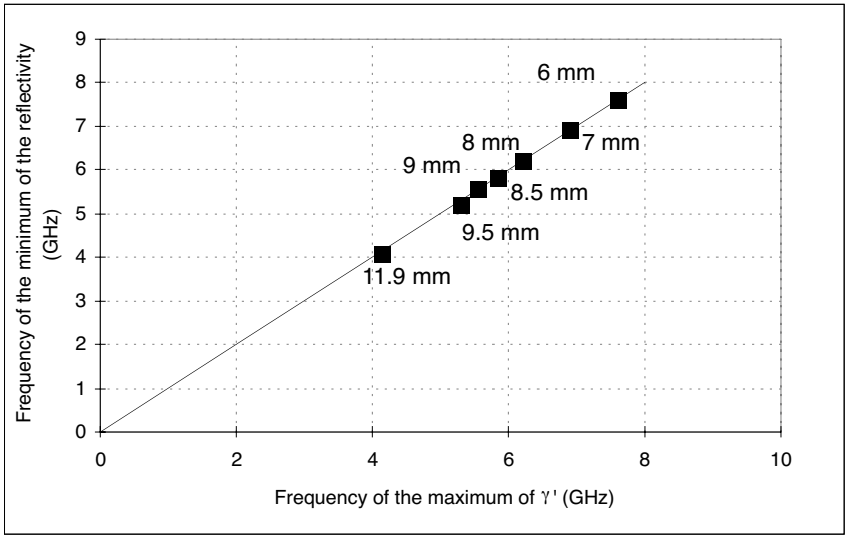

Figure 17. Period array 15 mm, Dielectric layer thickness is 3 mm, $\varepsilon_r = 5.81 + 1.82i$.

mode, for several patches sizes. Two quantities are almost perfectly correlated, with a correlation coefficient equals to 0.995. It suggests that the absorption of an electromagnetic wave by a screen combining a Dällenbach absorber with a periodic array of metallic patches may be due to a resonance in the surface wave excited by the metallic array and guided by the dielectric layer.

Moreover, the frequency of this maximum of absorption, depending on the patches dimensions, also depend of the other characteristics of the structure like the dielectric permittivity, and the thickness of the homogeneous layer.

5. CONCLUSION

In this paper we have studied the propagation of surface (or guided) waves in an absorbing structure consisting of a metal-backed dielectric layer with doubly periodic metallizations on its surface. Such structures have been shown to be thin and broadband electromagnetic absorbing screens [8, 13, 14].

The study of the propagation constant of the surface waves has been performed by considering the pole of the reflection coefficient location in the complex plane. To do this, we have defined an extended version of the moment method usually employed for the

reflection coefficient computation. This new method accepts complex incident propagation constants and includes the necessary two-sheeted definition of the complex $z^{1/2}$ function. Then it has been connected to a numerical method, which computes the zeroes of complex functions and based on the argument principle and Müller's algorithm. So we have calculated zeroes of the inverse of the reflection coefficient rather than directly compute the poles of the reflection coefficient, which is of course equivalent.

Starting with the simplest case where the periodic metallization is absent, the introduction of the array of patches was considered like a perturbation of the initial structure. The result was a continuous modification of the propagation constants of the surface wave guided by the metal-backed slab, which have been first calculated. Then a parametric study of the propagation constants was done with respect to the dielectric losses into the layer, the patch size, the period of the array. The frequency was regarded as an external parameter.

A main result was the observation that the pole trajectory may cross the branch cut of the two-sheeted complex plane and then move to the second Riemann sheet (Fig. 13) for a relevant configuration of the patch array and angle of incidence. So the structure is then capable to absorb completely an incident electromagnetic wave under a so-called called a Brewster angle.

Another interesting result was the correlation shown in Figure 17 between the frequencies of the maximum of γ' and the minimum of the reflectivity of the structure when illuminated by a plane wave at normal incidence. This shows that the maximum of the electromagnetic absorption occurs when the excitation of the surface waves in the structure is resonant.

REFERENCES

1. Collin, R. E., *Field Theory of Guided Waves*, Chapter 11, McGraw-Hill Book Company, Inc., New York, 1960.
2. Goubau, G., "Surface waves and their application to transmission lines," *Journal of Applied Physics*, Vol. 21, 1119–1128, November 1950.
3. Attwood, S. S., "Surface wave propagation over a coated plane conductor," *J. Applied Physics*, Vol. 22, 504–509, 1951.
4. Ling, R. T., J. D. Scoller, and P. Ya. Ufimtsev, "The propagation and excitation of surface waves in an absorbing layer," *Progress In Electromagnetic Research*, PIER 19, 49–91, 1998.

5. Felsen, L. B. and N. Marcuvitz, *Radiation and Scattering of Waves*, Prentice-Hall, Inc., 1973.
6. Jacobsen, J., "Analytical, numerical, and experimental investigation of guided waves on a periodically strip-loaded dielectric slab," *IEEE Transactions on Antennas and Propagation*, Vol. AP-18, No. 3, 379–388, May 1970.
7. Berginc, G., C. Bourrely, C. Ordenovic, and B. Torresani, "A numerical study of absorption by multilayered biperiodic structure," *Progress in Electromagnetic Research*, J. A. Kong (ed.), PIER 19, 199–222, EMW Publishing, Cambridge, Massachusetts, USA.
8. Terracher, F. and G. Berginc, "A broadband dielectric microwave absorber with periodic metallizations," *Journal of Electromagnetic Waves and Applications*, Vol. 13, 1725–1741, 1999.
9. Felsen, L. B. and N. Marcuvitz, *Radiation and Scattering of Waves*, Chapter 5, Fields in Plane-Stratified Regions, Sec. 5-6, Prentice-Hall, Inc., Inglewood Cliffs, N. J., 1973
10. Chabat, B., *Introduction à l'Analyse Complexe*, Tome 1, Fonctions d'une variable, Mir and Moscou (eds.), 1990.
11. Burke, J. J., "Propagation constants of resonant waves on homogeneous, isotropic slab waveguides," *Applied Optics*, Vol. 9, No. 11, 2444–2452, November 1970.
12. Richmond, J. H., L. Peters, Jr., and R. A. Hill, "Surface waves on a lossy planar ferrite slab," *IEEE Transactions on Antennas and Propagation*, Vol. AP-35, No. 7, 802–808, July 1987.
13. Terracher, F. and G. Berginc, "Thin electromagnetic absorber using frequency selective surfaces," *Proc. 2000 IEEE AP-S International Symposium*, 846–849.
14. Sha, Y., K. A. Jose, C. P. Neo, and V. K. Varadan, "Experimental investigation s of microwave absorber with FSS embedded in carbon fiber composite," *Microwave and Optical Technology Letters*, Vol. 32, No. 4, February 20, 2002.